A Multiple Baseline Interferometric Radar for Multiple Target Angular Velocity Measurement

Jason Merlo[©], Graduate Student Member, IEEE, Eric Klinefelter[©], Graduate Student Member, IEEE, Stavros Vakalis[©], Graduate Student Member, IEEE, and Jeffrey A. Nanzer[©], Senior Member, IEEE

Abstract—We present a novel technique for directly estimating the angular velocities of multiple targets using multi-baseline millimeter-wave interferometric radar to significantly reduce nonlinear signal distortion caused when multiple targets are present. We show that through the multiplication of the normalized instantaneous frequency measurements across different baselines, nonlinear intermodulation products resulting from dual-antenna interferometric angular velocity measurements can be mitigated, producing only the terms corresponding to the angular velocity of the targets in the scene. To validate this, simulations were performed demonstrating the close agreement between the proposed method and an ideal correlation (without intermodulation distortion). Near-field errors resulting from far-field approximations are analyzed. Finally, experimental results of a three-antenna, three-baseline 38-GHz interferometric radar are presented that demonstrate the recovery of the motion of two oscillating pendulums of differing angular frequencies.

Index Terms—Interferometric distortion mitigation, interferometric radar, millimeter-wave radar, multi-target angular velocity estimation.

I. INTRODUCTION

ESTIMATION of the velocity of remote targets is critical for many radar systems. Utilizing this information, the radar system may leverage a large class of tracking algorithms to refine position estimates over time, as well as predict the position and velocity, or state, of a target into the future [1]. However, beyond simply estimating and predicting target locations, velocity information of a target can be used for activity classification through the estimation of micro-motion parameters [2] and has subsequently been applied to problems such as pedestrian activity classification [3] and hand gesture classification [4]. Recent advancements have also demonstrated the ability to make direct angular velocity measurements through the use of correlation interferometry by leveraging the time-varying phase information at two spatially distributed apertures [5], which has further been applied to tangential micro-motion classification [6], [7].

Modern radar systems measure target range, radial velocity, and angle. Recently, it was shown that a correlation interferometer adds a fourth basic direct radar measurement of

Manuscript received February 16, 2021; revised April 13, 2021; accepted May 9, 2021. Date of publication May 12, 2021; date of current version August 9, 2021. (Corresponding author: Jeffrey A. Nanzer.)

The authors are with the Department of Electrical and Computer Engineering, Michigan State University, East Lansing, MI 48824 USA (e-mail: merlojas@msu.edu; klinefe4@msu.edu; vakaliss@msu.edu; nanzer@msu.edu).

Color versions of one or more figures in this letter are available at https://doi.org/10.1109/LMWC.2021.3079842.

Digital Object Identifier 10.1109/LMWC.2021.3079842

angular velocity [5]. However, when multiple targets of differing angular velocities are present, there exist intermodulation distortion (IMD) terms occurring from the mixing product between responses from differing targets at each antenna; the ideal response only produces the mixing product between scattered signals from the same target at each receiver. The intermodulation between multiple targets produces a frequency that is proportional to the difference in the radial velocities of different targets and has no meaningful physical interpretation. Several approaches have previously been proposed to mitigate these effects such as using very long wavelength carriers to make the Doppler shift negligible, producing only the desired frequency at the output of the interferometer, or using short pulses to eliminate intermodulation from radially separated targets [8]. Another approach utilizes the inverse radon transform as a specialized method of reducing this unwanted distortion when observing the position of rotating blades [9]. Recently, a more general method was proposed using a uniform linear array to sum the conjugate of adjacent baselines to cancel the phase of intermodulation products [10].

We present a novel technique for mitigating the distortion of multiple moving targets in an interferometric radar angular velocity measurement by using a multiple baseline interferometer array. Through the use of diverse baseline distances, the baseline-normalized frequency corresponding to the desired angular velocity remains constant across all baselines, while the IMD is spread arbitrarily on each baseline. This allows for the intermodulation products to be efficiently mitigated by simply multiplying the baseline-normalized frequency spectra from each baseline, similar to estimating target angles in multiplicative arrays [11] and the interferometric technique used for directly measuring multiple target angles with a modulated carrier waveform [12].

II. MULTI-BASELINE DISTORTION MITIGATION

The baseband response at the output of a single baseline of an M baseline correlation interferometer, shown in Fig. 1, in the presence of N targets can be found by correlating the received signals at the two antennas of baseline m

$$r_{Dm} = \langle r_{d1}^{(m)} \cdot r_{d2}^{*(m)} \rangle$$

$$= \left\langle \sum_{n} e^{j2\pi f_0 \tau_{1,n}^{(m)}} \cdot \sum_{n} e^{-j2\pi f_0 \tau_{2,n}^{(m)}} \right\rangle$$
(1)

where $r_{d1}^{(m)}$ and $r_{d2}^{(m)}$ are the baseband signals from the first and second receivers in the *m*th baseline, $\tau_{1,n}^{(m)}$ and $\tau_{2,n}^{(m)}$ are the

1531-1309 © 2021 IEEE. Personal use is permitted, but republication/redistribution requires IEEE permission. See https://www.ieee.org/publications/rights/index.html for more information.

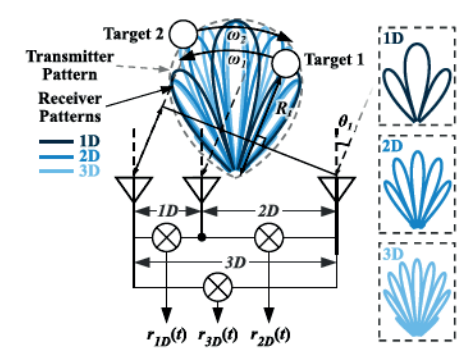


Fig. 1. Schematic of an M=3 baseline interferometer. Transmitter and downconversion mixers are not shown. The interference patterns generated by each baseline are shown in blue. Different baselines will have a different number of grating lobes dependent on their respective electrical distances.

round-trip time delays of the signal from the transmitter to the nth target, back to receivers 1 and 2 of the mth baseline, and ⟨·⟩ indicates time averaging. Because of the multiplication of all N targets in (1), the resulting terms will contain differential delays from the same scatterer at each antenna which are denoted $\tau_{1,n}^{(m)} - \tau_{2,n}^{(m)} = \Delta \tau_{gn}^{(m)}$, as well as differences between the reflected signal at different targets. As is illustrated in Fig. 1, the time difference between received signals from the same scatterer, n, at different antennas can be represented as the geometric time delay of a plane-wave impinging on the array, and thus can be represented as $\Delta \tau_{gn}^{(m)} = (D_m/c) \sin \theta_n$. However, there will be an additional N(N-1) unwanted terms which correspond to the intermodulation between the scattered signals from differing targets at each antenna in the baseline. In general, the angular velocity of the targets determine the instantaneous frequency of (1), which can be found by taking the time derivative of its phase term. The ideal instantaneous frequency from the nth target, without IMD, is

$$f_n^{(m)} = \frac{d}{dt} \frac{D_m}{c} \sin(\theta_n) = \omega_n D_{\lambda m} \cos(\theta_n) \tag{2}$$

where ω_n is the angular velocity of the *n*th target, $D_{\lambda m}$ is the length of the *m*th baseline in wavelengths, and the time derivative operates on $\theta_n = \omega_n t$ [5]. Finally, if θ_n is small, the small angle approximation can be used, thus $\omega_n = f_n^{(m)}/D_{\lambda m}$.

To remove the N(N-1) unwanted intermodulation terms, we propose a time-frequency matrix-based approach. First, we generate a time-frequency matrix representation of the signal from each baseline by taking the magnitude of the short-time Fourier transform of the signal, then normalize the frequency axis of each baseline matrix by its length in wavelengths $D_{\lambda m}$, and finally apply the Hadamard product across all baselines to achieve a multi-baseline time-frequency product (MBP) matrix

$$\mathbf{S}_{\mathsf{MRP}} = \mathbf{S}_{1D} \circ \mathbf{S}_{2D} \circ \dots \circ \mathbf{S}_{MD} \tag{3}$$

where S is the magnitude of the short-time Fourier transform. Note that after frequency normalization, all fundamental responses reside at the same frequency. Upon multiplication, the magnitude of the fundamental terms is scaled by M. The intermodulation products, which do not depend on $D_{\lambda m}$, will

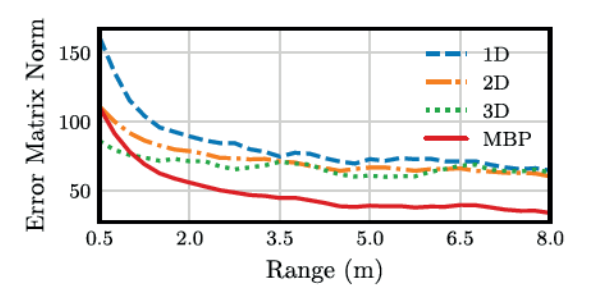


Fig. 2. Norm of the simulated error matrix versus average target range for each baseline and the MBP. In the near-field, the relationship between the interferometric frequency shift and angular velocity is nonlinear, thus the norm of the error of the MBP is higher.

be scaled arbitrarily and suppressed after multiplication. Note that we choose the baselines to be even multiples of *D* for simplicity, however, increased baseline diversity will generally improve IMD mitigation by providing greater intermodulation product frequency separation.

III. SIMULATION

The multi-baseline approach was evaluated in simulation by modeling the responses of two-point targets oscillating within the field of view of an array with $D=10.71\,\lambda$ and $f_0=38\,\mathrm{GHz}$, as shown in Fig. 1. Each target oscillated sinusoidally, tangentially to the array, while the average target distance was varied from 0.5 to 8 m. To quantify the reduction of the IMD, we define a matrix norm of the error between the magnitudes of each baseline matrix and the ideal matrix as

$$||E|| = \frac{1}{N_f N_t} \left\{ \sum_{i=1}^{N_f} \sum_{j=1}^{N_t} [\log(|\mathbf{S}|) - \log(|\mathbf{S}_{\text{gt}}|)]^2 \right\}$$
(4)

where N_f is the fast Fourier transform size, N_t is the number of time samples, S is from the individual baselines, or the MBP, and $S_{\rm gt}$ is the corresponding ideal ground truth matrix. The ideal matrix is computed by correlating each target with itself only, and thus contains no nonlinear distortion terms. A plot of the error matrix norm versus average target range is shown in Fig. 2, showing the benefit of the MBP. As the targets move far-field to the array, the linear relationship between angular velocity and interferometric frequency shift improves the performance.

IV. EXPERIMENTAL EVALUATION

The this radar used for experiment consisted continuous-wave (CW) transmitter and direct-downconversion receivers spaced 1-D and 2-D apart (shown in Fig. 3) where $D = 84.6 \,\mathrm{mm}$ or $10.71 \,\lambda$ at 38 GHz. The transmitter consisted of a 19-GHz local oscillator signal transmitted from a Keysight FieldFox at 5 dBm, split four ways (one for transmit, three for receive), then doubled in frequency and amplified by an analog device (ADI) HMC6787A active upconverter and amplified by a 24.5-dB ADI HMC7229 power amplifier before being transmitted from a 15-dBi 3-D printed horn antenna. The three receivers utilized the same 15-dBi antennas followed by ADI HMC1040 23-dB low-noise amplifiers and ADI HMC6789B downconverters.

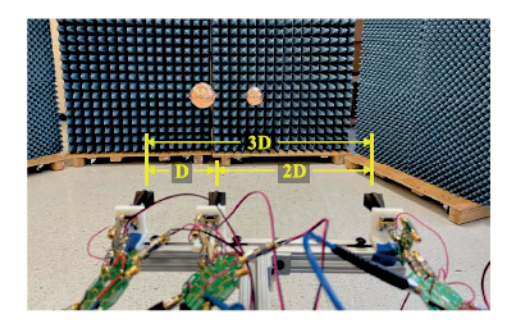


Fig. 3. Experimental measurement configuration. The three baselines of 1-D, 2-D, and 3-D are in the foreground while the two swinging spherical copper pendulums are suspended by clear wire in the background. The transmitter horn antenna is located below the cross-bar in the center of the array.

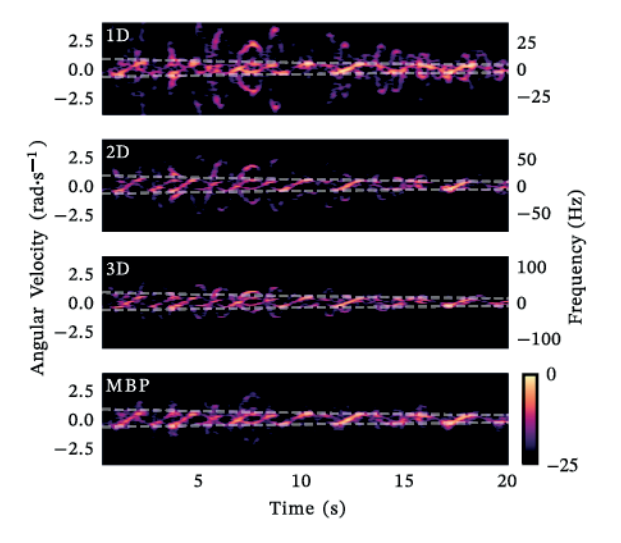


Fig. 4. Measured responses to two oscillating pendulums with 25-dB dynamic range (color scale near MBP applies to all plots). The oscillations of the pendulums start out of phase and end in phase. Dashed lines represent the envelope of the desired oscillations. In the individual baseline measurements, the fundamental frequencies are largely masked by IMD. Upon multiplication the resultant response is principally the fundamental frequencies, validating the multi-baseline approach.

Finally, the baseband in-phase and quadrature signals were sampled by an NI USB-6002 DAQ at 4.167 kSps.

The experiment (see Fig. 3) consisted of swinging two pendulums made of polystyrene foam balls coated in copper tape and suspended from above at $R_1 = 1.49 \,\mathrm{m}$ and $R_2 = 1.67 \,\mathrm{m}$ using clear plastic wire of differing lengths - this allowed the pendulums to oscillate at different frequencies causing the motion to move in and out of relative phase as is seen in Fig. 4. The measured time-frequency responses of the 1-D, 2-D, and 3-D baselines and the MBP are shown in Fig. 4; a 1-D time-slice at t = 7.6 s detailing the relative power levels of the intermodulation on each baseline is shown in Fig. 5. Exponentially decaying envelopes (dashed gray lines) were fit to the signal in the MBP to show the detection of the desired signal envelope. A periodic change in received power is present in both oscillations. These are due to a slight offset of the interferometer to one side of the oscillation which caused more power to be received during the half of the oscillation with positive acceleration due to the high gain antennas; additionally, the rear pendulum experienced minor shadowing by the sphere in the foreground. In the

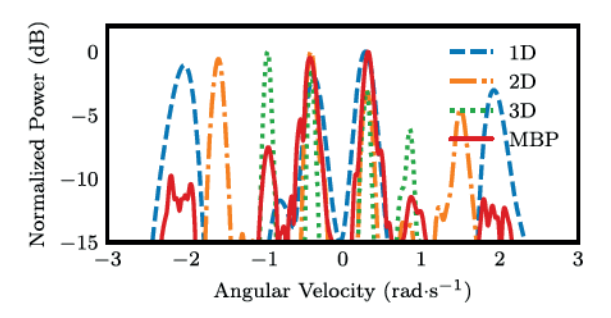


Fig. 5. Time slice of the power spectral density of the 1-D, 2-D, 3-D, and MBP measurements taken at t = 7.6 s. A reduction of several dB can be seen in all intermodulation products producing prominent peaks only at the true angular velocity values near ± 0.5 rad \cdot s⁻¹.

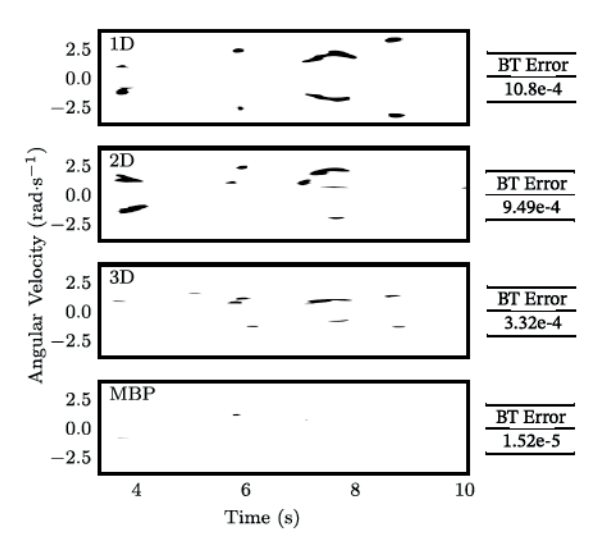


Fig. 6. Binary threshold (BT) error data showing all time-frequency cells outside the pendulum signal envelope with normalized power levels above -10 dB (left), normalized sum of thresholded cells (right). While the resolution improves as D increases creating thinner intermodulation bands, the intermodulation is still clearly present on each individual baseline.

measured case, perfect ground-truth knowledge of the scene is not available, thus another metric had to be defined. To quantify the effect of the performance of the MBP compared to the constituent baselines, a binary threshold (BT) error metric was implemented which sums all time-frequency bins outside the oscillation frequency envelope with power levels above -10 dB (see Fig. 6), normalized by the sum of the total number of time-frequency bins in the matrix. For the 1-D, 2-D, and 3-D baselines, errors of 10.8e-4, 9.49e-4, and 3.32e-4 resulted. For the MBP, the error was 1.52e-5, more than an order of magnitude less than any individual baseline.

V. CONCLUSION

A novel method for the mitigation of nonlinear IMD in correlation interferometers in the presence of multiple dynamic targets has been presented. Through the use of multiple unique baseline distances, the intermodulation products on individual baselines may be significantly attenuated using a simple multiplication operation enabling low-complexity systems to directly measure the angular velocity of multiple targets using low-cost CW radar hardware.

REFERENCES

- S. S. Blackman, Multiple-Target Tracking with Radar Applications. Norwood, MA, USA: Artech House, 1986.
- [2] V. C. Chen, F. Li, S.-S. Ho, and H. Wechsler, "Micro-Doppler effect in radar: Phenomenon, model, and simulation study," *IEEE Trans. Aerosp. Electron. Syst.*, vol. 42, no. 1, pp. 2–21, Jan. 2006.
- [3] Y. Kim and T. Moon, "Human detection and activity classification based on micro-Doppler signatures using deep convolutional neural networks," *IEEE Geosci. Remote Sens. Lett.*, vol. 13, no. 1, pp. 8–12, Jan. 2016.
- [4] T. Fan et al., "Wireless hand gesture recognition based on continuouswave Doppler radar sensors," *IEEE Trans. Microw. Theory Techn.*, vol. 64, no. 11, pp. 4012–4020, Nov. 2016.
- [5] J. A. Nanzer, "Millimeter-wave interferometric angular velocity detection," *IEEE Trans. Microw. Theory Techn.*, vol. 58, no. 12, pp. 4128–4136, Dec. 2010.
- [6] J. A. Nanzer and K. S. Zilevu, "Dual interferometric-Doppler measurements of the radial and angular velocity of humans," *IEEE Trans. Antennas Propag.*, vol. 62, no. 3, pp. 1513–1517, Mar. 2014.

- [7] H. Liang, X. Wang, M. S. Greco, and F. Gini, "Enhanced hand gesture recognition using continuous wave interferometric radar," in *Proc. IEEE Int. Radar Conf. (RADAR)*, Apr. 2020, pp. 226–231.
- [8] J. A. Nanzer and K. S. Zilevu, "Distortion mitigation in interferometric angular velocity measurements," *Electron. Lett.*, vol. 50, no. 18, pp. 1316–1318, Aug. 2014.
- [9] X. Wang, P. Wang, and V. C. Chen, "Simultaneous measurement of radial and transversal velocities using interferometric radar," *IEEE Trans. Aerosp. Electron. Syst.*, vol. 56, no. 4, pp. 3080–3098, Aug. 2020.
- [10] P. Wang, H. Liang, X. Wang, and E. Aboutanios, "Transversal velocity measurement of multiple targets based on spatial interferometric averaging," in *Proc. IEEE Int. Radar Conf. (RADAR)*, Apr. 2020, pp. 709–713.
- [11] V. G. Welsby and D. G. Tucker, "Multiplicative receiving arrays," J. Brit. Inst. Radio Engineers, vol. 19, no. 6, pp. 369–382, Jun. 1959.
- [12] S. Vakalis and J. A. Nanzer, "Millimeter-wave angle estimation of multiple targets using space-time modulation and interferometric antenna arrays," 2020, arXiv:2008.00356. [Online]. Available: http://arxiv.org/abs/2008.00356